EXPERIMENTAL INVESTIGATION OF SEPARATING FLOW IN A PLANE ASYMMETRIC DIFFUSER

Olle Törnblom, Björn Lindgren & Arne V. Johansson
Department of Mechanics,
Royal Institute of Technology,
Osquarsbacke 18, SE-100 44 Stockholm, Sweden.
olle@mech.kth.se, oso@mech.kth.se & viktor@mech.kth.se

ABSTRACT

The flow in a plane asymmetric diffuser has been studied experimentally and compared to an explicit algebraic Reynolds stress model (EARSM) computation (Gullman-Strand (2002)). The inlet flow is fully developed turbulent channel flow and a separation bubble is formed on the inclined wall. The mean separation and reattachment points are found, in the experiment, at 9 and at 31 inlet channel heights respectively. The model under-predicts the size of the separation bubble, this is attributed to an over-estimation of the wall normal turbulence component in a region close to the diffuser inlet. By analyzing the balance between the production and dissipation of turbulence kinetic energy we find that the predicted dissipation is too large. Hence, a better model for the production term in the transport equation for the turbulence time-scale-determining quantity (*e.g.* ε or ω) might be a key to better agreement.

INTRODUCTION

Separation is common in many fluid flow applications. Therefore it is important to improve the understanding of such flows and to develop methods of preventing separation by means of flow control. One such flow where we often encounter separation is the diffuser flow. This is often due to a practical need for rapid expansion of the diffuser cross section area, implying a large positive pressure gradient in the streamwise direction which may lead to separation of the diffuser wall boundary layers.

The aim of this project is to determine the characteristics of a separated plane asymmetric diffuser flow, to provide a reliable data-base for the turbulence modelling community of such a flow and to identify flow mechanisms that can be used in future schemes for efficient separation control. In this report we will limit ourselves to evaluating measurement data for quantities that are particularly interesting in turbulence modelling. The aim here is to compare the results of an explicit algebraic Reynolds stress model (EARSM) computation with the experimental data, and try to analyze where the model can be improved. The calculations were made by Lic. Johan Gullman-Strand from KTH, and are based on the code presented in Gullman-Strand (2002).

The plane asymmetric diffuser used in this study has one inclined wall with an opening angle of 8.5°. The opposite wall is straight, see figure 1. In the experiment the diffuser is preceded by a 3.2 m long channel with a height of 30 mm and a width of 1525 mm. This ensures fully developed turbulent channel flow as inlet condition (see *e.g.* Comte-Bellot (1965)). When computations and experiments are compared it is of the utmost importance to have the same, well defined, inlet conditions. Therefore, the fully developed turbulent channel flow was chosen since it is also easily produced in the calculations. In the experiment the diffuser is followed by a 2.5 m long outlet channel which is 141 mm high and 1525 mm wide. The purpose is here to minimize upstream influence from disturbances generated further downstream.

The primary measurement techniques used are Particle Image Velocimetry (PIV) in the streamwise wall-normal plane and Laser Doppler Velocimetry (LDV) in the spanwise direction. An advantage of these measurement techniques is that they can measure both direction and speed of particles following the flow, which is necessary when measurements are performed in the separated region. The measurement section comprises a short part of the inlet channel, the diffuser and part of the outlet channel, see figure 1. The velocity components were measured in the xy-plane at the spanwise center of the diffuser. The PIV measurements had a point separation of 1-2 mm in both directions depending on where the measurements were performed. The LDV measurements consist of 29 profiles across the diffuser at the spanwise centerline. All the measurements were then interpolated onto a common grid with a resolution of 10 mm in the streamwise direction and 2 mm in the wall-normal direction.

The Reynolds number based on the inlet channel height and the friction velocity of the channel flow was 2000. The sketch in figure 1 gives the dimensions of the diffuser. The end walls at the downstream end of the inlet channel are perforated and suction is applied to remove the end wall boundary layers and thereby prevent them from separating.

Flows in similar geometries (plane asymmetric diffusers) have previously been studied experimentally by *e.g.* Obi *et al.* (1993*a*), Obi *et al.* (1993*b*), Obi *et al.* (1997), Buice & Eaton (2000*a*) and Buice & Eaton (2000*b*). The opening angle of the diffuser was in all these studies slightly larger (10°). The reason for choosing a smaller diffuser opening angle in this project was to reduce the size of the separated region, and thereby, in combination with a high aspect ratio of the diffuser, achieve a high degree of two-dimensionality of the mean flow and moderate unsteadiness of the separation and reattachment points. Brunet *et al.* (1997) have also investigated a plane asymmetric diffuser flow, but in a geometry with much larger radius of the corners and another expansion ratio than in this study and the other studies mentioned above. In the studies by Obi *et al.* (1993*a*) and Brunet *et al.* (1997) the experiment were complemented by calculations using an Reynolds stress model (RSM) and a $k-\varepsilon$ approach, respectively.

Simulations and model prediction studies on the geometry with 10° opening angle have also been performed. An extensive numerical study of the plane asymmetric diffuser flow was made by Kaltenbach *et al.* (1999), who performed a Large Eddy Simulation (LES) at a Reynolds number of

1000 based on the inlet channel height and the inlet friction velocity. Their data showed good agreement with the experimental data by Buice & Eaton (2000*a*) for mean velocity profiles. The location of the separation point also agreed well but some discrepancy with the experimental data was found in the location of the reattachment point. A possible reason for this can be the relatively small spanwise width of the computational domain which may tend to artificially enhance spanwise coherence of large scale structures. Kaltenbach *et al.* (1999) found that the sub-grid scale model plays an essential role to calculate the flow correctly, since sub-grid stresses give a major contribution to the wall-shear stress. The sub-grid scale model must also adapt to the increase in turbulence level in the downstream part of the diffuser.

Numerical studies involving more or less advanced closures based on eddy-viscosity models, (differential) Reynolds stress models and EARSM models have been performed by a number of research groups. For instance, Apsley & Leschziner (1999) tested a number of linear and non-linear eddy viscosity models as well as differential stress-transport models. They found that strain dependent coefficients and anisotropy resolving closures are needed. However no models tested were capable of resolving all flow features in the diffuser. Apsley & Leschziner (1999) also point out the possibility to encounter problems related to the "flapping" motion of the unsteady separation. In an Ercoftac workshop (Hellsten & Rautaheimo (1999)), different numerical approaches with varying turbulence models were tested and compared to the Buice & Eaton (2000*a*) data-base. Models used comprised $k-\varepsilon$, $k-\omega$, RSM and LES. The agreement was, for the more simple models, in general fairly poor indicating that more complex models are needed to capture the complex flow in the diffuser. More recently Okinaga & Obi (2000) studied the importance of the models near-wall treatment. Their conclusion was that it is more important to predict the anisotropy behavior correctly than the wall asymptotics.

The plane asymmetric diffuser has also been used as a test case for commercial codes. The investigation performed by Iaccarino (2000) aimed at finding the limits of the versatile commercial codes in this complex geometry. The codes tested were CFX, Fluent and Star-CD. Two turbulence models were tested, ($k-\varepsilon$ and $\overline{v^2}-f$) in these three codes. The results were compared to the Obi *et al.* (1993*a*) and Buice & Eaton (2000*a*) data-bases. The $k-\varepsilon$ model was unable to capture the recirculation zone but the $\overline{v^2}-f$ model did so with an accuracy in separation length of 6%. The agreement for the friction coefficient was also fairly good.

As is seen above, an ample amount of numerical tests of closures in plane asymmetric diffusers exists already today but some of the major challenges in turbulence modelling are still related to near-wall turbulence and pressure-gradient induced separation. Phenomena which are represented in an ideally generic manner in the plane asymmetric diffuser flow. The present choice of opening angle ensures a separation-free flow along the straight wall, and the aspect ratio together with end-wall boundary layer control measures ensure a high degree of spanwise uniformity. The smaller opening angle also increases the modelling challenge because the flow is now quite close to be fully attached which makes it harder to predict the mean separation and reattachment points. (Fully attached flow occur for opening angles around 7°.) To conclude, this makes the present case ideal for detailed tests of turbulence modelling aspects that may require a high degree of accuracy in the turbulence statistics to evaluate differences in modelling approaches among high-level single-point closures, and sub-grid scale models in the LES-approach. The presently created data-base, containing information on all velocity components and related second order statistics, would, for instance, be well suited for tests of modern non-linear RSM:s and newly developed approaches, including curvature corrections etc, within the concept of EARSM.

EXPLICIT ALGEBRAIC REYNOLDS STRESS MODELS

A straightforward way to generalize the standard eddy-viscosity based two-equation model approach, is to introduce the transport equations for the Reynolds stresses

$$\frac{DR_{ij}}{Dt} = \mathcal{P}_{ij} - \varepsilon_{ij} + \Pi_{ij} + \mathcal{D}_{ij}. \tag{1}$$

Such a model is referred to as a differential Reynolds stress model (DRSM) and pioneering work on this type of model was made by Launder *et al.* (1975). From equation 1 an equation for the Reynolds stress anisotropy tensor can be derived. This tensor is defined as

$$a_{ij} \equiv \frac{\overline{u_i' u_j'}}{K} - \frac{2}{3}\delta_{ij}. \tag{2}$$

Assuming that the flow is in so called "weak equilibrium" the advection and diffusion terms in the transport equation for the anisotropy tensor can be discarded. Weak equilibrium means that the timescale on which the anisotropy relaxes to some quasi-equilibrium state prescribed by the mean flow and the turbulent scales is small (see *e.g.* Rodi (1976)). If the pressure-strain rate and dissipation rate anisotropy are modelled in terms of the mean strain rate (S_{ij}), the mean rotation rate (Ω_{ij}), a_{ij} and the turbulence velocity and length scales (*e.g.* K and ε), the weak equilibrium assumption implies that the Reynolds stress anisotropy is completely determined by the local values of the mean strain and rotation rate tensors (normalized by the turbulence time scale), *i.e.*

$$f_{ij}(\mathbf{a}, \mathbf{S}^*, \mathbf{\Omega}^*) = 0. \tag{3}$$

Equation 3 represents an implicit relation between the anisotropy tensor ($\mathbf{a}$) and the normalized strain ($\mathbf{S}^*$) and rotation rate ($\mathbf{\Omega}^*$) tensors. The weak equilibrium assumption does not hold in slowly distorted turbulence where $\mathcal{P}/\varepsilon \ll 1$, *e.g.* in the outer part of a boundary layer or in the center of a jet or a channel-flow.

Using the weak equilibrium assumption together with an isotropic assumption for the dissipation rate tensor and

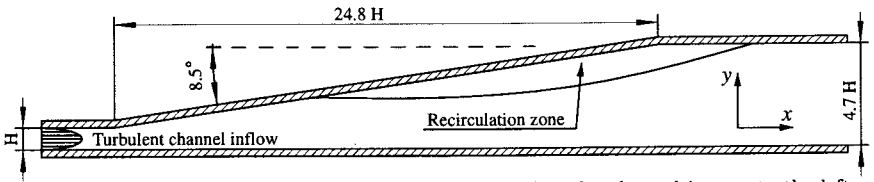

Figure 1: The measurement section of the wind-tunnel. A part of the inlet channel is seen to the left and part of the outlet channel is seen to the right.

linear model for the pressure strain rate tensor one can derive an explicit algebraic equation for the anisotropy (see *e.g.* Gatski & Speziale (1993) and Wallin & Johansson (2000)), *i.e.*

$$a_{ij} = a_{ij}(\mathbf{S}^*, \mathbf{\Omega}^*). \tag{4}$$

Such an expression requires very little effort to be evaluated, so the increase in computational effort for an EARSM compared to a standard two-equation model is almost negligible. The explicit expression is also a good way of ensuring robustness of the computational scheme.

The EARSM has several advantages over an ordinary eddy-viscosity based two-equation model, where

$$a_{ij} = 2C_\mu S^*_{ij}. \tag{5}$$

The EARSM has been shown to improve near-wall behavior and thereby reduce the need for near-wall damping, as compared to eddy-viscosity models. Effects of system rotation and streamline curvature can also be captured in the EARSM:s through extensions analyzed by *e.g.* Girimaji (1997) and Wallin & Johansson (2002). This correction is based on a formal derivation of the weak equilibrium assumption in a streamline orientated curvilinear co-ordinate system. The corrections introduced are fully three-dimensional and Galilean invariant and vanishes in flows without curvature or rotation effects.

NUMERICAL METHOD

The model prediction results included in the present paper have been obtained using a finite element code solver created by an automated code generation procedure, described in Amberg *et al.* (1999). The system of equations are the Reynolds averaged Navier-Stokes (RANS) equations and the Wallin & Johansson (2002) EARSM combined with the Wilcox low-Re $K-\omega$ formulation. The RANS equations were solved in a time-dependent fractional step scheme described by Guermond & Quartapelle (1997) and a decomposition of the inverse turbulence time-scale, ω, into an outer part and a near wall part with the correct near wall behavior ($\omega = \tilde{\omega} + \omega_w$) decreased the demand of grid resolution close to the walls. A more detailed description of the code generation procedure, formulation of the equations and solution strategy can be found in Gullman-Strand (2002).

The geometry used in the computations was identical to the one in the experiment with respect to diffuser angle and inlet to outlet height ratio but with inlet and outlet lengths of 10 x/H and 60 x/H respectively and with an infinite spanwise length. The inlet flow condition was generated by an auxiliary simulation of fully developed turbulent channel flow according to the guide-lines of Hellsten & Rautaheimo (1999) and the outlet flow condition was constant pressure parallel flow and zero velocity gradient in the streamwise direction. The mesh consisted of structured triangular elements with 318 nodes in the streamwise direction, of which 100 were located in the diffuser and 75 nodes stretched in the wall-normal direction. See Gullman-Strand (2002) for further details.

RESULTS

In this results section the focus is on a comparison between the measured and the calculated data but first the streamlines and the back-flow coefficient are presented to provide an understanding of the size and character of the separation bubble on the inclined wall.

Stream-function

The stream-function is here defined as

$$\Psi(x,y) = 1 - \frac{1}{HU_\mathrm{b}} \int_0^y U(x,y)\mathrm{d}y. \tag{6}$$

In figure 2, constant values of the stream function (streamlines) are plotted throughout the measurement region. This definition of the stream function gives a value of $\Psi = 0$ at the dividing streamline. The dividing streamline separates the (averaged) recirculation zone from the outer flow. The two positions where the dividing streamline reaches the "upper" wall are the mean separation and reattachment points, respectively. From figure 2, the mean separation point is found to be located at 9 channel heights downstream the diffuser inlet ($x/H \approx 9$) and the mean reattachment point is located at $x/H \approx 31$.

In figure 2 the gray-scale levels represent a measure of the speed in the diffuser, *i.e.* here $\sqrt{U^2+V^2}$, with an increment of 2 m/s. The figure shows how the flow with maximum velocity first is deflected at the inlet corner towards the inclined wall but when it approaches the separation point it bends back towards the straight wall. Thereafter, there is a very slow relocation of the maximum towards the center of the outlet channel. It can also be noted that the decrease in speed is slower through the diffuser compared to an attached flow case. This follows from the constriction caused by the separated region, which decreases the adverse pressure gradient and slows down the retardation of the flow speed and spreads it out over a larger downstream length.

Back-flow coefficient

A very interesting quantity is the back-flow coefficient (χ) which relates the number of samples with negative velocity (along the inclined wall) to the samples with positive velocity. A back-flow coefficient of 1 means that all samples have negative velocity and a back-flow coefficient of zero thus means that all samples have positive velocity. The back-flow coefficient then reads

$$\chi(x,y) = \frac{1}{2N}\sum_{k=1}^{N}(1- \\ -\mathrm{sgn}(u_k(x,y)\cos(\alpha) + v_k(x,y)\sin(\alpha))), \tag{7}$$

where N is the total number of samples, sgn is the sign function, u_k the x-component of the velocity in the k^{th} sample, v_k the y-component of the velocity in the k^{th} sample and $\alpha = 8.5°$ the diffuser opening angle.

First, we notice in figure 3 that along the straight wall there seems to be no samples with back-flow although the rather poor resolution might allow for a very thin separation bubble very close to the wall. It is important that there is no separation on the straight wall since this may destroy the "stability" of the separation bubble on the inclined wall. The opening angle chosen, 8.5° is thus small enough to avoid this kind of flow state.

Focusing our attention on the separation bubble on the inclined wall the back-flow coefficient gives us the streamwise locations on the inclined wall for the most upstream instantaneous separation point that in figure 3 is shown to be $x/H \approx 5$. The flow is separated 80% of the time downstream $x/H \approx 14$. In real time the separation point moves back and forth along the inclined wall and at some occasions the flow is completely attached. A back-flow coefficient of 0.5 gives the mean separation point, already shown to be

$x/H \approx 9$ from the dividing streamline, and the mean reattachment point at $x/H \approx 31$. The reattachment point never moves downstream of $x/H \approx 35$ where the flow thus always is attached.

Comparison with the model predictions

Model predictions from a Wallin & Johansson (2000) EARSM are here compared to our experimental data. Most of the previously tested turbulence models (*e.g.* Hellsten & Rautaheimo (1999) and Apsley & Leschziner (1999)) have underestimated the size of the separated region and this is also the case in this computation.

In figure 4 a comparison is made between the experimental separation bubble and the computed. It can be noted that the mean separation point is almost the same in the computation as in the experiment (although this is hard to see in the figure since the computed bubble is very thin near the separation point). The computed reattachment point is located at $x/H \approx 27$ which is approximately $4H$ upstream of point measured in the experiments. The height of the bubble is maybe even more important to correctly predict as the bubble size directly determines the character of the outer mean flow.

In figure 5 the streamwise (along the straight wall) velocity is shown. It can be seen that the qualitative shape of the profiles agrees rather well but the strength of the back flow is under-predicted which leads to a displacement of the maximum velocity towards the inclined wall and also a smaller velocity gradient in the wall normal (perpendicular to the straight wall) direction.

In figure 6 the variance of the fluctuation components is shown. In the upstream part of the diffuser the agreement is reasonably good for all components with the exception of the predicted wall-normal component ($\overline{v'^2}$), which is too large. There is reason to believe that this error contributes the smaller separation in the computation, *i.e.* the momentum transfer in the wall-normal direction is exaggerated in the computation.

The turbulence kinetic energy K in figure 7 is in rather close agreement in the the two most upstream profiles. Further downstream, in the region where we have separation, the agreement between experimental and computed profiles begin to deteriorate. The turbulence model is not capable of predicting the high turbulence levels in the exit channel. On the other hand, the computed production rate of K

$$\mathcal{P} = -\overline{u_i' u_j'} \frac{\partial U_i}{\partial x_j} \tag{8}$$

shown in figure 8 is larger than the experimental in the beginning of the diffuser but agrees fairly well further downstream. The level of turbulence kinetic energy is a balance between the production rate ($\mathcal{P}$) and the dissipation rate (ε) and in this case the dissipation rate must be over-estimated in the computation since K decrease faster in the computation than in the experiments, in the downstream direction. The over-estimation of the dissipation rate indicates that the modelling of the ε-equation could be made better. A good task for future research on anisotropy resolving two-equation models is, hence, to find better models for the production term in the transport equation for ε (in this case this the transport equation for ω).

ACKNOWLEDGEMENT

The Swedish Energy Agency and the Swedish Research Council are gratefully acknowledged for their financial support.

REFERENCES

Amberg, G., Törnhardt, R. & Winkler, C. 1999 Finite elemet simulations using symbolic computing. *Math. & Computers Sim.* **44**, 275–274.

Apsley, D. D. & Leschziner, M. A. 1999 Advanced turbulence modelling of separated flow in a diffuser. *Flow, Turbulence and Combustion* **63**, 81—112.

Brunet, L., Cazalbou, J. B., Chassaing, P. & Jervase, L. 1997 Experimental and computational study of pressure effects on turbulent flow in an asymmetric plane diffuser. In *11th Symp. on Turb. Shear Flows, Grenoble, France*, pp. 114–119.

Buice, C. U. & Eaton, J. K. 2000*a* Experimental investigation of flow through an asymmetric plane diffuser. *Tech. Rep.* TSD-107. Thermo sciences Division, Dep. of Mechanical Eng. Stanford University, Stanford, Ca, USA, Report No.

Buice, C. U. & Eaton, J. K. 2000*b* Experimental investigation of flow through an asymmetric plane diffuser. *J. of Fluids Eng.* **122**, 433–435.

Comte-Bellot, G. 1965 Écoulement turbulent entre deux paroix parallèles. Publications scientifiques et techniques 419. Ministère de l'air, 2, Avenue de la Porte-d'Issy, Paris.

Gatski, T. B. & Speziale, C. G. 1993 On explicit algebraic stress models for complex turbulent flows. *J. Fluid Mech.* **254**, 59–78.

Girimaji, S. S. 1997 A Galilean invariant explicit algebraic Reynolds stress model for turbulent curved flows. *Phys. Fluids* **9**, 1067–1077.

Guermond, J. L. & Quartapelle, L. 1997 Calculation of incompressible vicous flow by an unconditionally stable projection FEM. *Journal of Computational Physics* **132** (CP965587), 12–33.

Gullman-Strand, J. 2002 Turbulence modeling using automated code generation applied to asymmetric diffuser flow. Dept. of mechanics, KTH, Stockholm, Sweden, licentiate thesis.

Hellsten, A. & Rautaheimo, P., ed. 1999 *Workshop on refined turbulence modelling*. ERCOFTAC/IAHR/COST.

Iaccarino, G. 2000 Prediction of the turbulent flow in a diffuser with commersial CFD codes. *Tech. Rep.*. Center for Turbulence Research.

Kaltenbach, H. J., Mittal, M., Fatica, R., Lund, T. S. & Moin, P. 1999 Study of flow in a planar asymmetric diffuser using large-eddy simulation. *J. Fluid Mech.* **390**, 151–185.

Launder, B., Reece, G. & Rodi, W. 1975 Progress in the development of a Reynolds-stress turbulence closure. *J. Fluid Mech.* **41**.

Obi, S., Aoki, K. & Masuda, S. 1993*a* Experimental and computational study of turbulent separating flow in an asymmetric plane diffuser. In *9th Symp. on Turbulent Shear Flows, Kyoto, Japan, August 16-18*, p. 305.

Obi, S., Ishibashi, N. & Masuda, S. 1997 The mechanism of momentum transfer enhancement in periodically perturbed turbulent separated flow. In *2nd Int. Symp. on Turbulence, Heat and Mass Transfer, Delft, The Netherlands*, pp. 835–844.

Obi, S., Ohizumi, K. & Masuda, S. 1993*b* Turbulent separation control in a plane asymmetric diffuser by periodic perturbation. In *Engineering Turbulence Modeling and Experiments 2*, pp. 3633–642.

Okinaga, Y. & Obi, S. 2000 Effect of near-wall treatment on the prediction of turbulent separating flows. In *4th JSME-KSME Thermal Engineering Conference, Kobe, Japan, Oct. 1-6*.

Rodi, W. 1976 A new algebraic relation for calculating the Reynolds stresses. *Z. argew. Math. Mech.* **56**, T219–221.

Wallin, S. & Johansson, A. V. 2000 An explicit algebraic Reynolds stress modell for incompressible and compressible turbulent flows. *J. Fluid Mech.* **403**, 89–132.

Wallin, S. & Johansson, A. V. 2002 Modeling streamline curvature effects in explicit algebraic Reynolds stress turbulence models. *Int. J. of Heat and Fluid Flow.* **23**, 721–730.

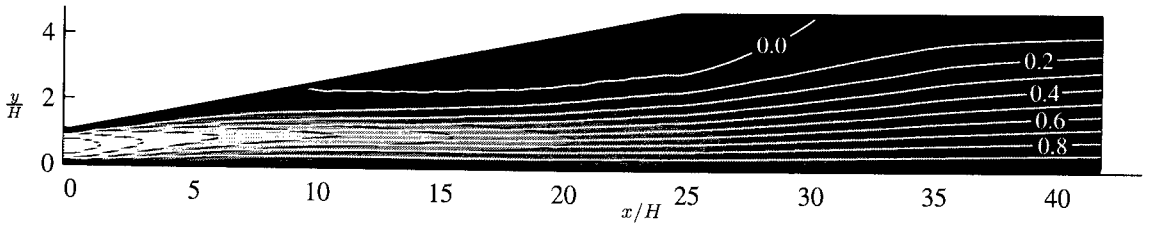

Figure 2: Streamlines ($\Psi(x, y)$) shown as white curves. The stream function is integrated from the inclined wall. Gray-scale background with separating black curves shows the speed, with a contour increment of 2 m/s.

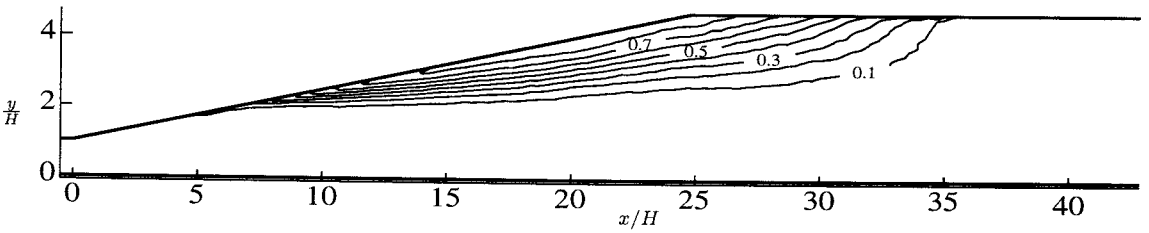

Figure 3: Back-flow coefficient, χ, defined along the inclined wall, χ.

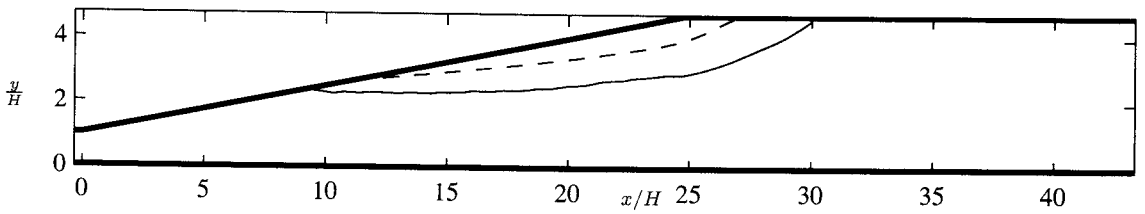

Figure 4: Dividing streamlines from experiment (−) and EARSM (−−).

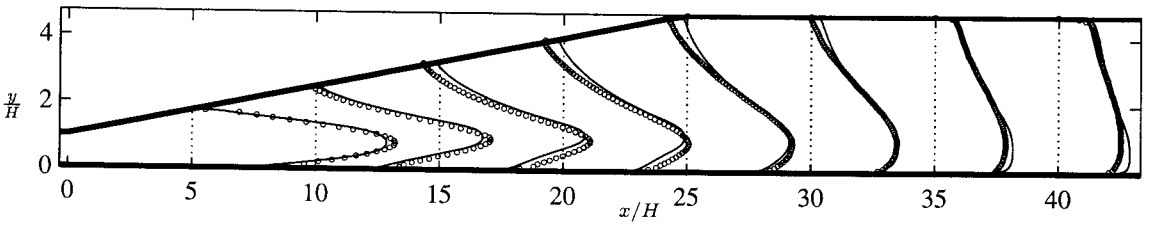

Figure 5: Streamwise velocity (parallel to the straight wall), $10U/U_b + x/H$. Experiments (o) and model predictions with (−) and without (−−) streamline curvature correction.

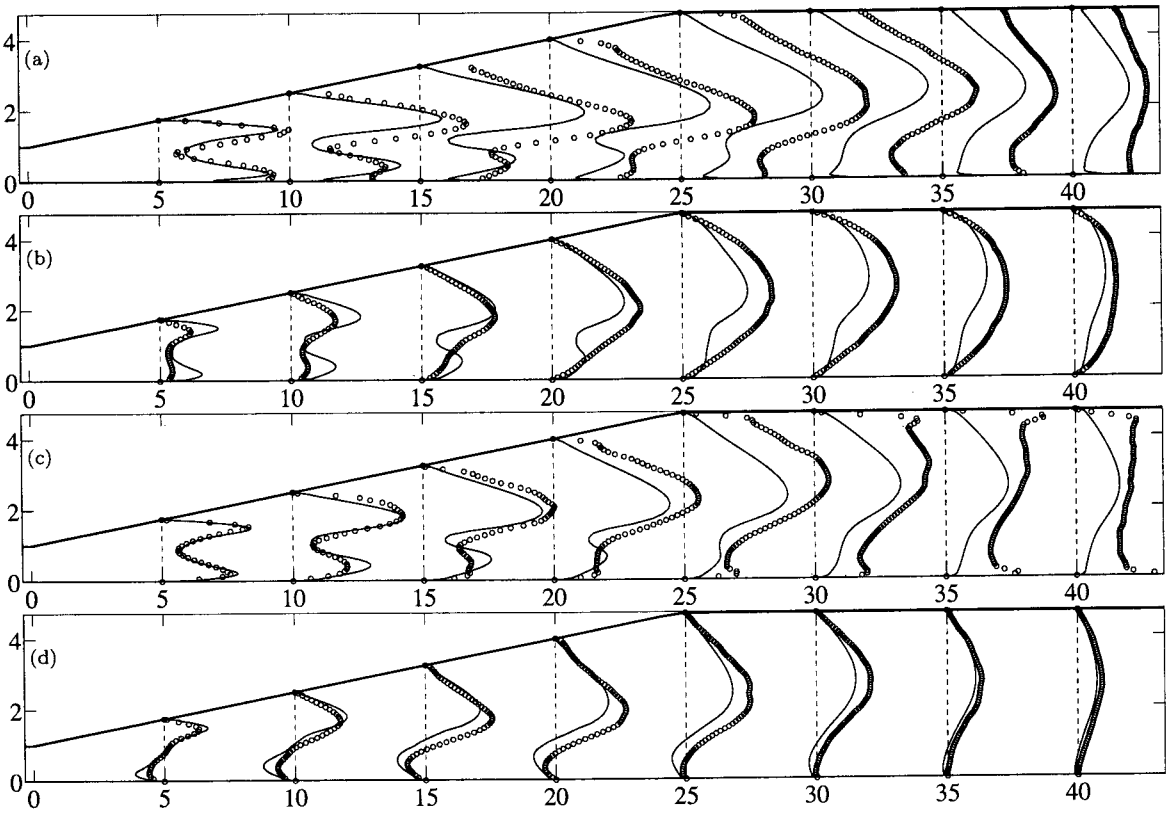

Figure 6: Measured (o) and computed (—) variance of turbulent fluctuations and Reynolds shear stress; (a) $\overline{u'^2}$, (b) $\overline{v'^2}$, (c) $\overline{w'^2}$ and (d) $\overline{u'v'}$, displayed as $500\frac{\overline{u_i'u_j'}}{U_b^2} + \frac{x}{H}$.

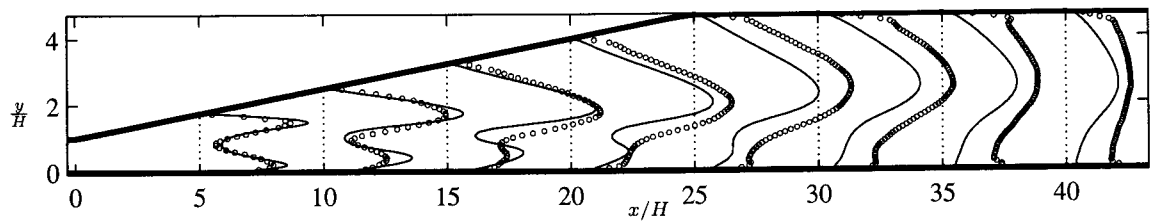

Figure 7: Turbulence kinetic energy, $400K/U_b^2 + x/H$. Experiments (o) and model predictions with (–) and without (––) streamline curvature correction.

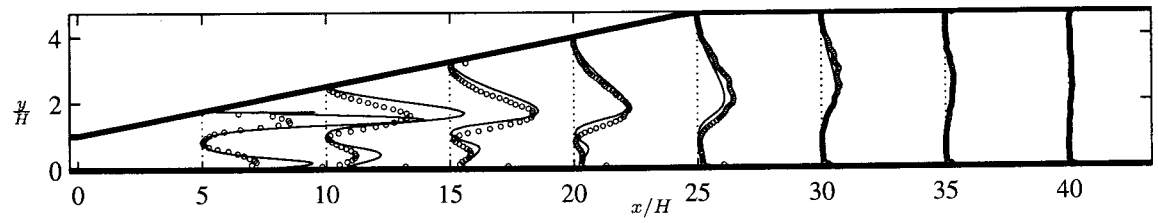

Figure 8: Production rate of turbulence kinetic energy ($1500\mathcal{P}H/U_b^3 + x/H$). Experiments (o) and model predictions with (–) and without (––) streamline curvature correction.